Solar Energy Materials & Solar Cells 297 (2026) 114124

Contents lists available at ScienceDirect

Solar Energy Materials and Solar Cells

journal homepage: www.elsevier.com/locate/solmat

# Thermal stability of laser-assisted fired TOPCon solar cells: Crucial insights for module manufacturing, certification testing, and field conditions

Xutao Wang [a], Jing Yuan [b], Jianjun Nie [b], Yan Zhu [a], Xiaoyan Zhang [b], Ting Gou [b], Daoxian Li [b], Weiguang Yang [b,*], Feng Li [b], Xinyuan Wu [a,**], Bram Hoex [a,***]

[a] School of Photovoltaic and Renewable Energy Engineering, University of New South Wales, Sydney, Australia, 2052
[b] Jolywood (Taizhou) Solar Technology Co., Ltd., Taizhou, Jiangsu, 225500, China

ARTICLE INFO

*Keywords:*
Laser-assisted firing
Thermal stability
TOPCon solar cell
Cell-to-module loss
$J_{02}$ recombination
Contact degradation

ABSTRACT

Laser-assisted firing (LAF) technology, such as laser-enhanced contact optimization (LECO), is increasingly utilized in the mass production of tunnel oxide passivated contact (TOPCon) solar cells. However, concerns regarding the thermal stability of LAF TOPCon remain. This study systematically evaluates the thermal stability of LAF TOPCon cells at both the moderate temperatures encountered during module fabrication and a higher temperature of 450 °C. While soldering did not have a negative impact on cell performance, lamination resulted in a ~0.29 % absolute power conversion efficiency (*PCE*) loss, primarily due to a reduction in fill factor (*FF*). The degradation is driven mainly by an increase in $J_{02}$-like recombination, likely in the space charge region. A 1-min one-sun light soaking at room temperature effectively restores cell performance, suggesting that field operation effectively mitigates such degradation. Under repeated 450 °C rapid thermal annealing and LAF cycles, initial *FF* and *PCE* losses (~21.6 % and ~6.7 % absolute, respectively) are attributed to contact deterioration, but performance is restored through subsequent LAF treatment. Based on these findings, a three-state defect model and contact degradation mechanisms are proposed. These findings provide new insights into the reliability of LAF TOPCon cells and highlight key considerations for industrial processing and module reliability testing.

## 1. Introduction

The Tunnel Oxide Passivated Contact (TOPCon) technology currently dominates the photovoltaic (PV) market, owing to a high power conversion efficiency (*PCE*) and low manufacturing costs. Based on the latest International Technology Roadmap for Photovoltaics (ITRPV) [1], the TOPCon technology now has a market share of ~60 % which is predicted to increase further in the next five years. Researchers and PV manufacturers are still pushing the boundaries of TOPCon technology, with significant progress reported recently [2–6]. The current world record efficiency for commercial large-size TOPCon solar cells is 26.4 % [7]. Despite the impressive advancements in TOPCon technology, further enhancing the *PCE* of TOPCon solar cells without sacrificing the reliability of PV devices remains a key focus for the PV industry.

In recent years, laser-assisted firing (LAF) techniques, such as laser-enhanced contact optimization (LECO), have attracted significant interest [8–11] and have already been widely adopted in TOPCon production lines [12,13]. The LAF process consists of a high-intensity laser scanning process on the front, combined with an applied reverse bias. The process induces localized heating at the metal–silicon interface, as the photogenerated current is confined to regions with initially relatively low contact resistance. This selective current flow leaves the remaining interface passivated by the dielectric stack, resulting in improved contact structure [14–19] and significantly higher *PCE* for TOPCon solar cells than those processed with a traditional single-step firing process. Our recent work [13] demonstrates that the utilization of LAF process can effectively reduce both front and rear contact recombination in TOPCon solar cells and lead to an increase in $V_{oc}$ of more than 10 mV. The enhancement in both efficiency and damp-heat stability was also successfully shown on commercial LAF TOPCon solar cells [12,20,21].

Nevertheless, some concerns remain regarding the stability of LAF TOPCon solar cells, particularly under thermal stress. Xie et al. [22]

* Corresponding author.
** Corresponding author.
*** Corresponding author.
*E-mail addresses:* yangwg01@jolywood.cn (W. Yang), xinyuan.wu@unsw.edu.au (X. Wu), b.hoex@unsw.edu.au (B. Hoex).

https://doi.org/10.1016/j.solmat.2025.114124
Received 24 August 2025; Received in revised form 22 October 2025; Accepted 12 December 2025

reported a severe contact issue when LAF TOPCon cells were subjected to a second high-temperature firing at temperatures above 500 °C. Notably, the *PCE* of their TOPCon solar cells reduced to only 1.15 % after a second firing at 680 °C, indicating that the LAF cells are highly thermally sensitive. Additionally, recent work [23] identified a new failure mode in LAF TOPCon solar cells, revealing that thermal stress at 400 °C combined with a reverse bias can significantly increase the contact resistance and result in a decrease of *PCE*. These findings suggest that certain thermal conditions can be extremely detrimental to LAF TOPCon solar cells. The conditions examined in these studies, particularly the high temperatures and applied reverse bias, are unlikely to occur after LAF in cell/module production lines or under normal operation conditions. However, they still provide valuable insight into the potential failure mechanisms of LAF cells. Therefore, to deepen the understanding of previously reported failure models, it is worth further investigating the thermal stability of LAF contacts, in particular for conditions experienced by the solar cell under module fabrication.

This work investigates the thermal stability of LAF TOPCon solar cells under both moderate and high-temperature conditions. Moderate thermal stress, which can be referred to as cell-to-module (CTM) loss after soldering and lamination, is simulated using a 10-s one-sun light soak at 350 °C and a 15-min dark anneal at 150 °C. A series of annealing and light soaking cycles was conducted to assess degradation and recovery behaviour. Notably, a 1-min one-sun light soaking at room temperature is found to effectively restore the performance after degradation, indicating that this thermal-induced CTM loss may be negligible for modules under real operation conditions. In addition, the stability of LAF cells under slightly higher temperatures was evaluated by subjecting samples to cycles of a rapid thermal annealing (RTA) process at 450 °C, followed by a LAF process. Based on the experimental results, a defect transformation model and refined mechanisms for contact deterioration are proposed to explain the thermal response of LAF cells under moderate and high thermal conditions.

## 2. Methodology

The structure of the TOPCon solar cells used in this work is shown in Fig. 1 (a). G10 (182.2 × 183.75 mm) n-type silicon substrates with a thickness of 130 μm and a resistivity of 1 Ω cm were used. All wafers were subjected to standard cleaning and alkaline texturing to form surface pyramids. Boron diffusion was employed to create the front-side $p^+$ homogenous emitter. On the rear side, a tunnelling $SiO_x$ layer and phosphorus-doped polycrystalline silicon ($n^+$ poly-Si) were grown using plasma oxidation and plasma-assisted *in situ* doping (POPAID). Surface passivation was completed with atomic layer deposited (ALD) $AlO_x$ and plasma-enhanced chemical vapor deposited (PECVD) $SiN_x$ layers on the front, and a PECVD $SiN_x$ layer on the rear. The commercial paste and laser-assisted firing (LAF) process were applied for solar cell metallization.

This study comprehensively investigates the thermal stability of LAF TOPCon solar cells under both moderate- and high-temperature stress. The moderate-temperature thermal test was conducted to assess cell-to-module (CTM) losses. Therefore, two key module fabrication steps, soldering and lamination, were selected as the test conditions. As shown in Fig. 1 (b), one group of cells underwent both processes, while another experienced only lamination for comparison. One-sun current-voltage (I-V) measurements were used to track performance after each step. To isolate thermal effects, soldering was applied without ribbons or flux, and lamination was conducted using only glass and fiberglass fabrics. To enhance experimental practicality in subsequent trials, soldering was emulated by a 10-s one-sun light soaking at 350 °C (actual peak temperature at 230 °C for 3 s), and lamination by a 15-min dark annealing at 150 °C. These conditions were validated to replicate the real thermal stress during module fabrication, using halogen lamps with a hotplate and a thermal oven, respectively.

Moreover, the high-temperature stability was evaluated by rapidly annealing samples at 450 °C (actual peak temperature at 430 °C for 3 s), followed by a LAF process. Additional cycles of RTA and LAF were conducted to assess repeatability, with one-sun I–V measurements recorded after each step as well.

The Suns-Voc and one-sun I–V measurements were performed using Sinton Instruments FCT650/750 I-V testers. Electroluminescence (EL) images were captured by an ASICCN SCSS EL tool. A BTi (LIS-R3) luminescence imaging system conducted photoluminescence (PL) measurement, with a high-$V_{oc}$ lens. Open-circuit PL images were taken under 1 sun, 0.1 sun, and 0.05 sun to evaluate injection-dependent

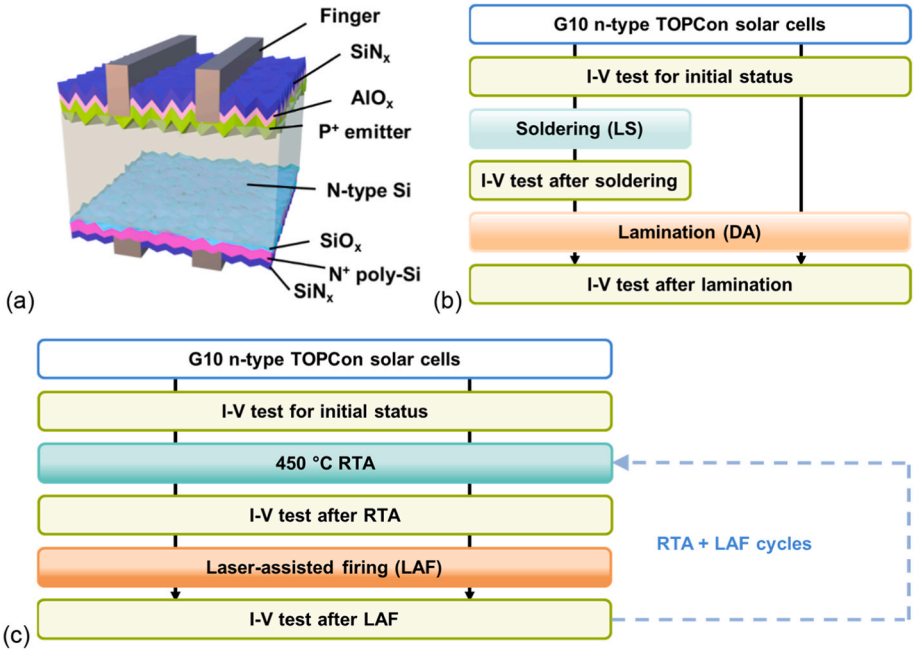


**Fig. 1.** (a) The schematic of the LAF TOPCon solar cell, as well as the experimental flow chart of the stability test (b) under the thermal conditions during soldering and lamination, and (c) under the high-temperature RTA and LAF cycles.

recombination, with exposure times scaled accordingly to ensure similar levels of PL counts. Short-circuit PL images were also acquired to locate recombination sites. All PL images were processed using ImageJ [24].

## 3. Results and discussions

### 3.1. CTM loss caused by thermal process

Fig. 2 illustrates the I-V parameters of LAF TOPCon solar cells under two different thermal conditions: soldering + lamination (blue-green line) and lamination only (orange line), as illustrated in Fig. 1 (b). Fig. 2 (a) shows that the samples that only underwent lamination exhibited a decline in *PCE* (~0.29 $\%_{abs}$), while the *PCE* of the soldering + lamination group increased slightly (~0.06 $\%_{abs}$) after soldering but then decreased significantly after lamination. Fig. 2 (c) and (d) shows a ~1.5 mV reduction in $V_{oc}$ and ~0.66 $\%_{abs}$ decrease in *FF* for the lamination group. Moreover, samples subjected to both soldering and lamination showed a moderate increase in $V_{oc}$ after soldering, which is potentially due to hydrogen passivation of preexisting defects during light soaking, but followed by a severe decrease after lamination. Like the $V_{oc}$, the *FF* of the soldering + lamination group also improved slightly after soldering, but then reduced significantly after lamination. However, the $J_{sc}$ of both groups shown in Fig. 2 (b) remains relatively stable, with only a minor decrease observed after the lamination process.

In summary, both groups exhibited consistent performance degradation after the lamination process, primarily due to the decrease in *FF*, followed by a smaller decline in $V_{oc}$. This indicates a potential CTM loss induced by the thermal stress associated with the lamination process. Additionally, the corresponding thermal performance of TOPCon cells produced without LAF technology is also provided in Section 3.5.1 to support the mechanism discussion.

### 3.2. Detailed analysis of moderate thermal stability

#### 3.2.1. I-V and Suns-$V_{oc}$ results under thermal process

Since the degradation was only observed during the lamination process, dark annealing tests at three different temperatures (150 °C, 180 °C, and 250 °C) were conducted to further investigate the thermal stability. Notably, the 150 °C dark annealing is a representative condition to emulate the actual lamination process.

After the 150 °C dark annealing test, the *PCE* of LAF TOPCon solar cells in Fig. 3 (a) initially reduced by ~0.28 $\%_{abs}$, followed by a gradual recovery. This can be attributed to $V_{oc}$ and *FF*, both of which exhibited similar degradation and recovery trends in Fig. 3 (c) and 3 (d), respectively. In contrast, $J_{sc}$ shown in Fig. 3 (b) remained relatively stable throughout the annealing duration. As discussed in Section 3.1, the degradation was primarily attributed to the loss of *FF*. Therefore, further analysis of the multiple electrical factors contributing to *FF* loss is presented. Fig. 3 (e) illustrates a slight increase in series resistance ($R_s$) during 150 °C dark annealing, likely related to the contact resistance at the sensitive metal-Si contact of LAF cells [22,23]. Additionally, the pseudo fill factor (*pFF*), shown in Fig. 3 (f), presented a degradation and recovery trend consistent with the curves of *PCE*, $V_{oc}$ and *FF*. Fig. 3 (g) compares the $\Delta FF$-$\Delta pFF$ (representing the $R_s$-induced *FF* loss) with the absolute change in *pFF* ($\Delta pFF$) after 150 °C dark annealing. The results indicate that the initial *FF* degradation can mainly be attributed to a reduction in *pFF*, while the impact of $R_s$ became more significant after ~240 min of dark annealing. Additionally, Fig. 3 (h) and (f) show $J_{01}$ and $J_{02}$, which were extracted from the Suns-$V_{oc}$ measurements using a double-diode model. Since $J_{01}$ primarily reflects recombination at a high-injection level, the observed increase and subsequent reduction showed good agreement with the trends of $V_{oc}$. Similarly, the performance of *pFF* could be primarily attributed to a change in $J_{02}$, which is more apparent in low minority carrier concentrations [25].

Samples annealed at higher temperatures (180 °C and 250 °C) exhibited similar degradation and recovery trends to those annealed at 150 °C. However, elevated temperatures significantly accelerated both the degradation and recovery processes and reduced the overall extent of degradation. These results suggest that degradation and recovery occurred simultaneously [26–28] and performed as competing mechanisms during dark annealing. By the end of the test, the $V_{oc}$ of samples annealed at 180 °C and 250 °C surpassed their initial values, consistent with the lower final $J_{01}$ value. During the 250 °C annealing, $J_{02}$ started to recover after just 2 min, leading to a full recovery of *pFF* by the end of the process. Notably, during the latter stages of annealing at 250 °C, the *PCE* exhibited a gradual degradation, primarily due to a reduction in *FF*,

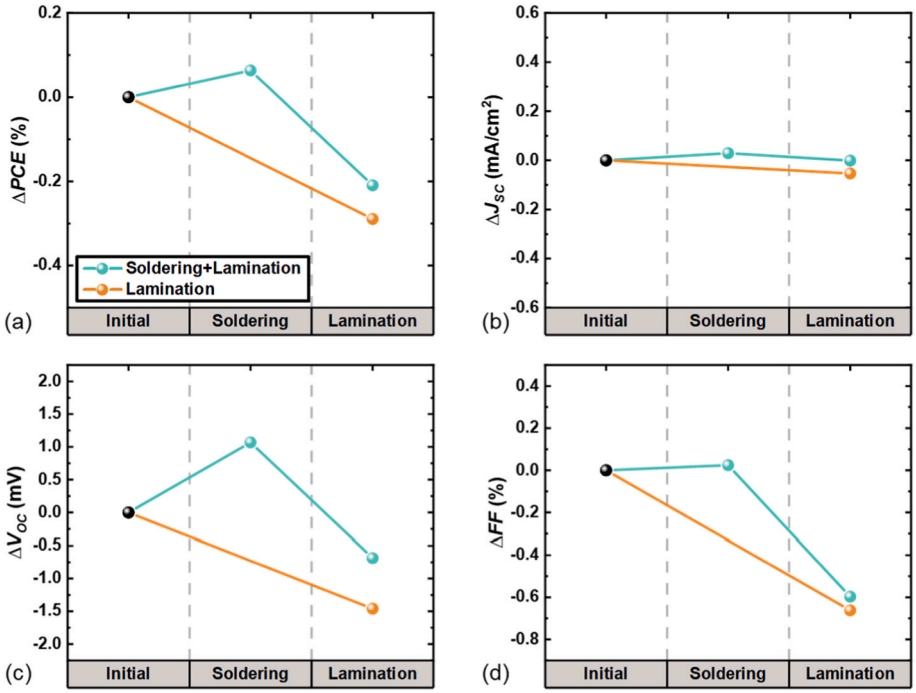


**Fig. 2.** Absolute variations of the one-sun (a) *PCE*, (b) $J_{sc}$, (c) $V_{oc}$, and (d) *FF* values of the TOPCon solar cells after the soldering and lamination process.

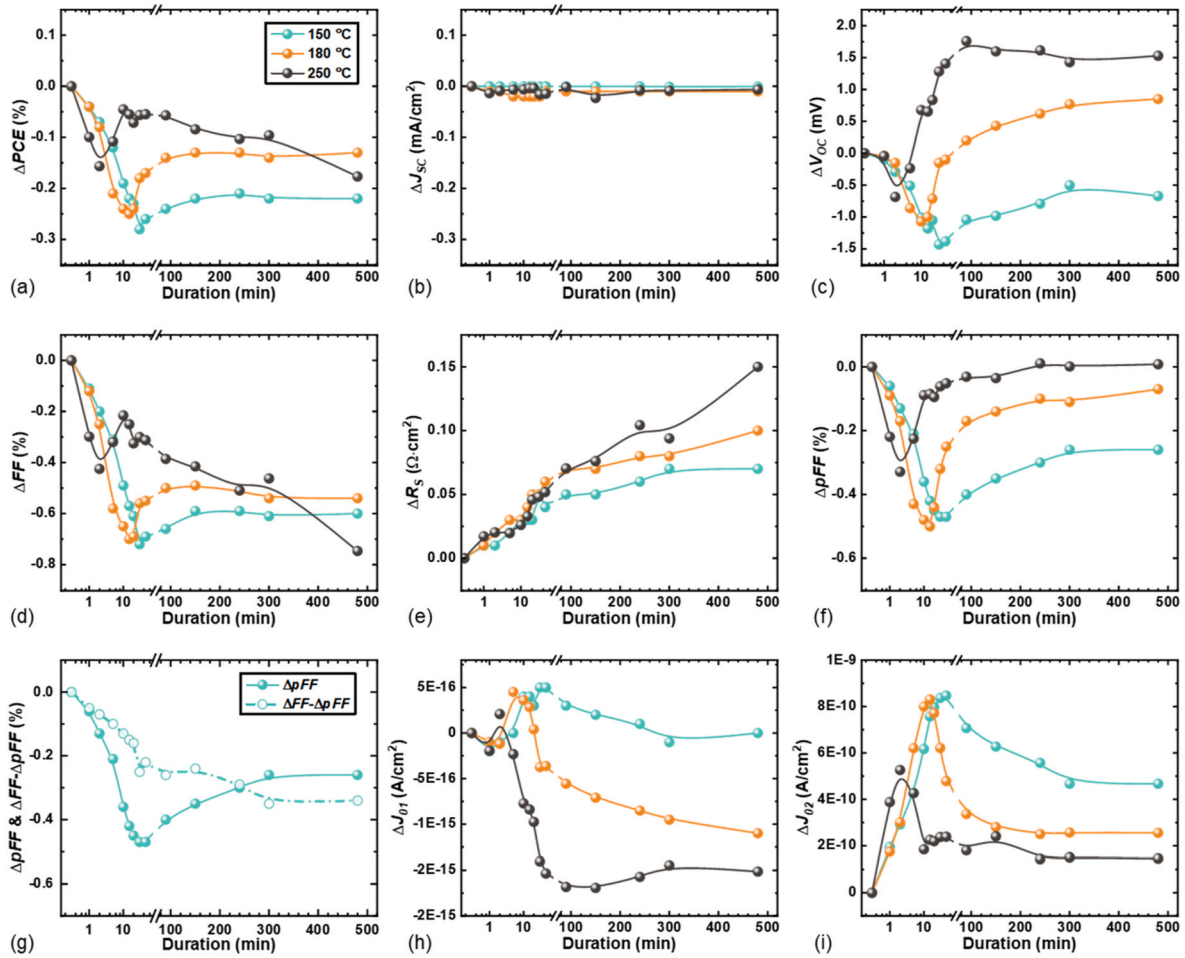


**Fig. 3.** Absolute variations of one-sun I-V parameters of TOPCon solar cells during dark annealing at 150 °C, 180 °C, and 250 °C, respectively.

which was caused by a faster increase in $R_s$ with extended annealing time.

In summary, the thermal degradation of LAF TOPCon solar cells during the lamination-like dark annealing process was primarily due to the *FF* loss, which was dominated by changes in *pFF*. The degradation in *pFF*, in turn, was mainly attributed to non-ideal ($J_{02}$-like) recombination, such as edge recombination [29–32] and space charge region (SCR) recombination [25,33]. Additionally, the apparent increase in the extracted $J_{02}$ may also be due to the injection-level dependence recombination in the bulk or at the silicon interfaces [34–36]. Therefore, it is necessary to investigate the sites of the recombination and the underlying mechanism responsible for the observed degradation.

### 3.2.2. *Open-circuit (OC) and short-circuit (SC) photoluminescence images*

As thermal degradation is primarily driven by carrier recombination, photoluminescence (PL) imaging was conducted to examine changes in effective carrier lifetime following 150 °C dark annealing. Open-circuit PL (OC-PL) images in Fig. 4(a) show minor degradation under 1 sun excitation intensity, but significantly lower lifetimes at lower injection levels (0.1 and 0.05 sun), indicating strong injection-dependent recombination. The differential images (Initial – Annealed) further confirm that the incremental recombination was highly injection-

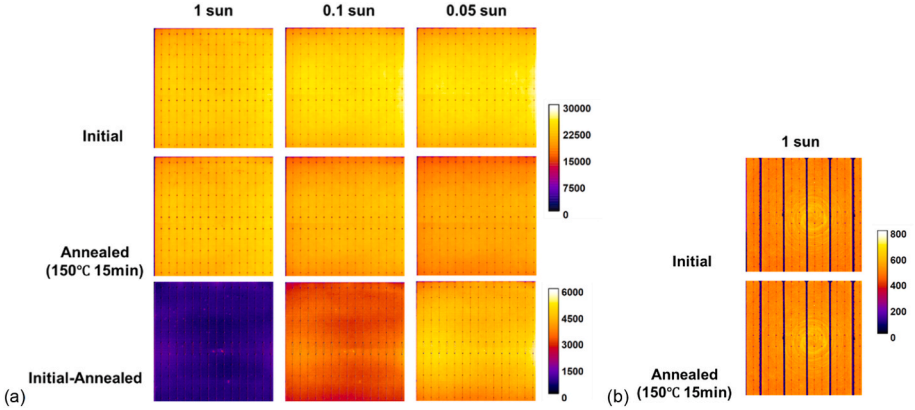


**Fig. 4.** (a) Open-circuit PL [at 1, 0.1, and 0.05 sun] and (b) short-circuit PL of TOPCon solar cells before and after 15 min dark annealing at 150 °C.

dependent, aligning with the $V_{oc}$ and *pFF* decrease observed in Fig. 3. The observed lifetime degradation across the whole cell suggests that edge recombination is not the primary cause.

To locate the recombination site, short-circuit PL (SC-PL) imaging was also performed. Since the minority carrier concentration at the edge of the p–n junction depends exponentially on the applied voltage [37], it becomes negligible at the front surface under short-circuit conditions. Consequently, the SC-PL image only reflects the carrier lifetime in the bulk and rear regions in our cells [38,39]. As shown in Fig. 4(b), no notable change (<1 % variation) was observed before and after annealing, indicating that degradation occurred predominantly in the front region—namely the front surface, emitter, and p–n junction. Combined with the increase in $J_{02}$ (Fig. 3), these results strongly suggest that space charge region (SCR) recombination is the primary cause of the observed degradation.

### 3.3. Effect of dark annealing and light soaking

To better understand the degradation and recovery behaviour, the changes in sample performance during the dark annealing and light soaking tests were systematically analyzed. The $V_{oc}$ and *pFF*, which are closely linked to the incremental recombination, were selected as the representative parameters in this study. 10-s 350 °C one-sun light soaking (LS) and 15-min 150 °C dark annealing (DA) treatments were employed to simulate the thermal conditions during the actual soldering and lamination process, respectively.

#### 3.3.1. Effect of dark annealing pretreatment

The results in Section 3.2.1 indicate that extended annealing the samples after the lamination process (simulated by a 15-min 150 °C dark annealing) or increasing the temperature of lamination could effectively minimize the CTM loss caused by the thermal stress. However, previous studies on light- and elevated temperature-induced degradation (LeTID) suggest that applying a pre-annealing treatment [40–43] prior to module assembly could be an effective approach to mitigating thermal degradation. In this work, the samples were pre-annealed at 250 °C for 15 min. As illustrated in Fig. 3, this process should enable the degradation and recovery cycle to be completed in advance without significantly sacrificing performance due to an increase in $R_s$.

Fig. 5 shows that a 15-min 250 °C DA process improved both $V_{oc}$ and *pFF*, likely due to the passivation of pre-formed defects in the sample after the metallization process. For the pre-annealed samples (Pre_DA), no significant degradation in $V_{oc}$ and *pFF* could be observed after the subsequent 15-min 150 °C DA (orange line), indicating the stabilizing effect of the 250 °C DA pretreatment. However, samples subjected to a 250 °C pre-annealing followed by a 10-s light soaking at 350 °C (Pre_DA + LS) exhibited a significant reduction in $V_{oc}$ and *pFF* after the 150 °C DA step (black line). Although the final performance of the Pre_DA + LS sample was slightly better than the reference sample (blue-green line), thanks to the temporary benefits of the 250 °C DA and 350 °C LS steps, significant *pFF* degradation still occurred after the whole process. Therefore, these results suggest that while 250 °C DA can initially stabilize defects, the subsequent soldering step may destabilize them, leading to "renewed" degradation during the lamination process.

#### 3.3.2. Dark annealing and light soaking cycles

Although the 250 °C pre-annealing step showed a stabilizing effect, it did not fully eliminate the CTM loss due to the reactivation of defects during the interval light soaking. This highlights the need to further investigate the underlying mechanisms. As a result, repeated test cycles were carried out, each consisting of a 15-min 250 °C dark annealing (DA), a 10-s 350 °C one-sun light soaking (LS), and a 15-min 150 °C DA. The changes in $V_{oc}$ and *pFF* during the corresponding process are shown in Fig. 6(a) and (b), respectively. The initial 150 °C DA led to ~2.2 mV reduction in $V_{oc}$, and ~0.5 $\%_{abs}$ decrease in *pFF*. This degradation was fully recovered by a subsequent 250 °C annealing, resulting in $V_{oc}$ and *pFF* values being even higher than their initial values. As explained earlier, this can be attributed to the passivation of some preexisting defects that were present after the metallization process. Afterwards, a 350 °C LS was applied to the samples to destabilize defects, followed by a second 150 °C DA, which again led to a degradation of both $V_{oc}$ and *pFF*. However, the relative degradation from the initial states was less severe than compared to the first 150 °C DA, indicating that at least parts of the passivated preexisting defects were not reactivated during the LS process. With the repetition of the cycles, the extent of both degradation and recovery was relatively consistent. Those results suggest that the light soaking process predominantly destabilized the defects passivated during the dark annealing process, rather than generating new active defect centers from a reservoir of recombination-inactive precursor state, as proposed in earlier studies [44].

#### 3.3.3. Possible solutions under operational conditions

Since the pre-annealing method could not fully resolve the CTM issue, the effect of a light soaking step after the lamination process was further investigated and plotted in Fig. 7. Consistent with previous results, both $V_{oc}$ and *pFF* showed a notable decline after the 150 °C DA. However, a 1-min one-sun light soaking at room temperature completely recovered the degradation, with $V_{oc}$ even exceeding its initial value. Subsequently, the samples were stored in a nitrogen box under dark conditions for 12 h. Interestingly, a degradation in $V_{oc}$ and *pFF* was observed, though the extent was smaller than that after the 150 °C DA. Repeating the LS process once more fully restored the parameters, and the degradation after the second dark storage cycle was even less pronounced than after the first.

These findings suggest that a brief light soaking treatment can effectively mitigate the CTM loss induced by the thermal stress during lamination, and thus, this CTM loss would not be apparent in field conditions. Despite the reversible degradation observed during dark

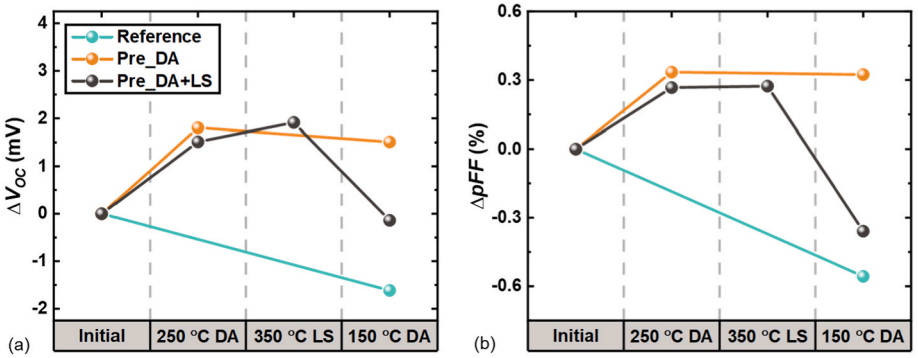


**Fig. 5.** The absolute variations in the one-sun (a) $V_{oc}$, and (b) *pFF* values of TOPCon solar cells after 250 °C dark annealing (DA) and/or 350 °C light soaking (LS) process, followed by a 15 min of 150 °C dark annealing.

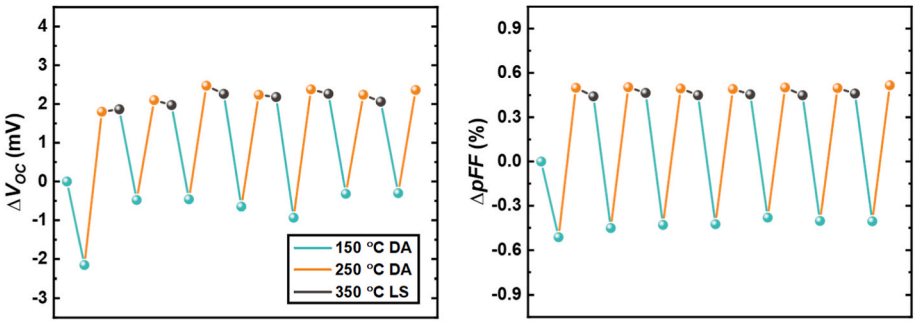


**Fig. 6.** Relative change in the (a) $V_{oc}$, and (b) *pFF* values for TOPCon solar cells subjected to 150 °C/250 °C dark annealing and 350 °C light soaking cycles.

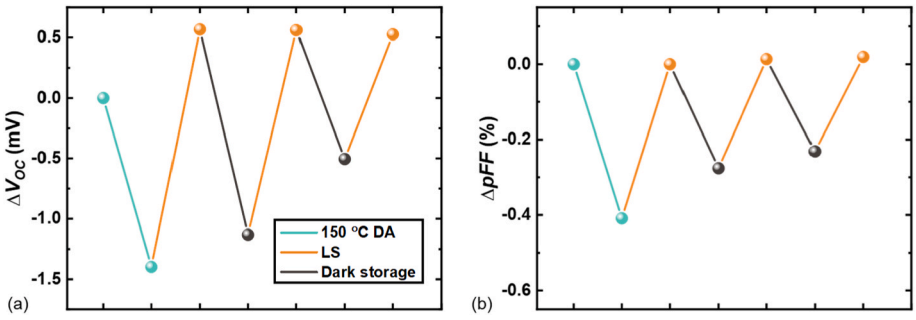


**Fig. 7.** Relative change in the (a) $V_{oc}$, and (b) *pFF* values for TOPCon solar cells under 150 °C dark annealing, light soaking and dark storage cycles.

storage, solar modules can readily self-recover upon exposure to sunlight. Interestingly, the recovery during light soaking and the degradation after dark storage closely resemble the behaviour observed in samples subjected to ultraviolet-induced degradation (UVID) light [45–47], suggesting a possible connection or similarity in the underlying mechanisms. These results underscore the importance of properly timing module characterization, especially for newly unpacked modules, to ensure measurements accurately reflect field performance under real operating conditions.

### 3.4. Degradation caused by high-temperature RTA

Apart from assessing the cell performance under moderate thermal conditions, this study also evaluates the stability of LAF cells under high-temperature RTA processes. Fig. 8 presents the one-sun I-V parameters of LAF TOPCon solar cells subjected to 450 °C RTA and LAF cycles, as outlined in Fig. 1 (c). As shown in Fig. 8 (a), a significant reduction in *PCE* (~6.7 $\%_{abs}$) could be observed on samples after a 450 °C RTA process. The degradation of the *PCE* could be primarily attributed to the remarkable ~21.6 $\%_{abs}$ reduction in *FF* in Fig. 8 (d), due to a rapid increase in series resistance ($R_s$). The slight reduction in $J_{sc}$ (~0.56 mA/

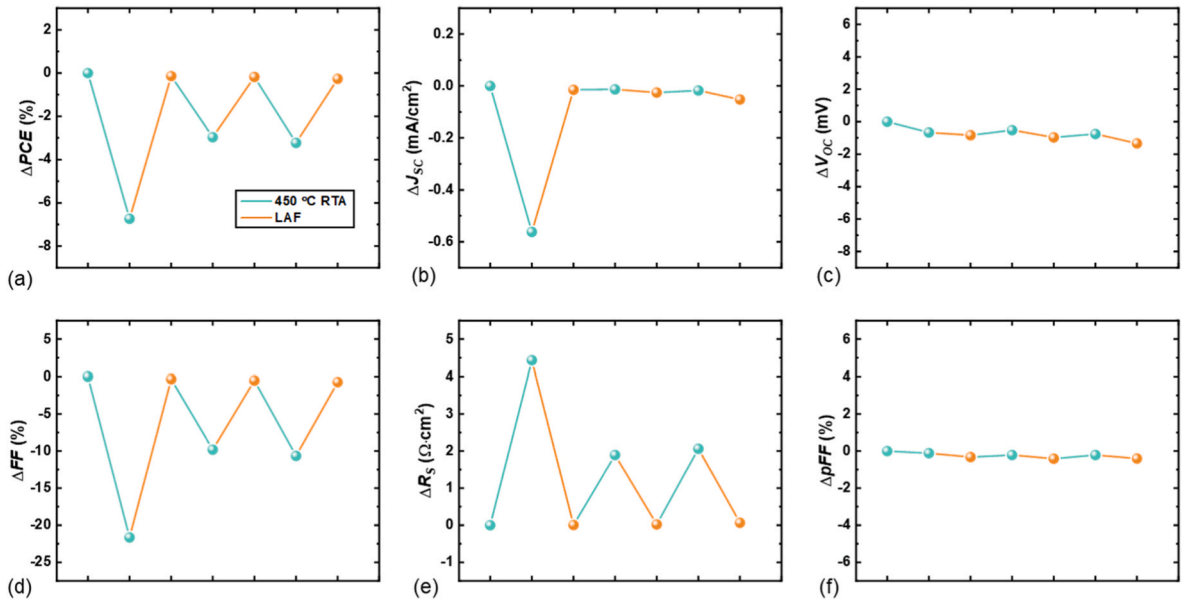


**Fig. 8.** Absolute variations of one-sun (a) *PCE*, (b) $J_{sc}$, (c) $V_{oc}$, (d) *FF*, (e) $R_s$, and (f) *pFF* values of TOPCon solar cells during the 450 °C RTA and LAF cycles, as outlined in Fig. 1 (c).

$cm^2$) also demonstrated a deterioration in carrier-collection ability after the RTA process. In contrast, both $V_{oc}$ and *pFF* remained relatively stable, suggesting no notable recombination loss.

A subsequent LAF process effectively recovered the $J_{sc}$, $R_s$ and *FF* of samples, thereby restoring the overall *PCE*. Those results align well with the previous finding [22] showing that high-temperature firing increases the contact resistance of LAF-formed contacts, which can be reversed by the LAF process. A second 450 °C RTA process again reduced the *PCE*, however, to a less extent of degradation. $J_{sc}$ remained nearly unchanged, and *FF* only decreased by ~9.8 $\%_{abs}$, due to the small increase in $R_s$. Afterwards, the overall performance could be recovered by the LAF process. Interestingly, a third 450 °C RTA process showed similar degradation to the second, while the subsequent LAF treatment could again restore the performance of samples.

The degradation of the metal-Si contact can also be evaluated by the EL images in Fig. 9. After the first RTA process, the EL image shows dark patterns, likely due to poor electrical contact. Moreover, the contact deterioration was less severe after the second and third RTA processes, which is consistent with the I-V results in Fig. 8. Therefore, the I-V and EL results suggest that the high-temperature RTA process induces deterioration of the metal-Si contact, resulting in a significant increase in $R_s$ and consequently a reduction in *FF*. However, this degradation can be effectively reversed through the LAF process. Notably, the degradation caused by the following RTA process is less serious, implying that the contact deterioration is not completely reproducible across the RTA and LAF cycles.

### 3.5. Proposed thermal stability mechanisms

#### 3.5.1. Hydrogen-related degradation

To the best of our knowledge, similar CTM losses caused by thermal degradation during lamination were not reported prior to the adoption of LAF technology. To explore the underlying mechanism, TOPCon solar cells fabricated using the LAF technique were compared with those fabricated using a traditional single-step baseline (BL) firing. Notably, the implementation of LAF has resulted in most TOPCon manufacturers eliminating the selective emitter (SE) from the front side. Fig. 10 presents the evolution of I-V parameters for samples with different emitter configurations processed using either LAF or BL technology. In this comparison, SE-BL refers to selective emitter precursors processed with the baseline metallization, while SE-LAF and HE-LAF correspond to selective emitter and homogeneous emitter (HE) precursors processed with a commercial LAF technique. The SE and HE precursors were carefully prepared to exhibit similar sheet resistance in the homogeneous regions, but the SE structures included additional localized high-level doping beneath the metal-Si contacts.

According to Fig. 10, a similar amount of *PCE* degradation was observed on both the SE-LAF and HE-LAF samples, primarily driven by the reduction in *FF* and $V_{oc}$. This suggests that the emitter configuration is unlikely to be the root cause of the induced degradation. In contrast, the SE_BL samples exhibited only minor degradation in *PCE* (~0.07 $\%_{abs}$), with significantly lower loss in both *FF* and $V_{oc}$. These results reveal that the corresponding thermal degradation during the module assembly is mainly associated with the utilization of the LAF technique.

Based on the characterization results, a three-state model, inspired by the one previously reported for BO-related degradation [48,49], is proposed in Fig. 11 to explain the sample behaviour under moderate thermal conditions. Notably, this model is used only as a conceptual framework to describe the activation and recovery dynamics of defects, rather than implying the involvement of boron–oxygen pairs in the degradation studied here. In this model, the inactive defects can be transitioned from the defect precursor state (State A) into a recombination-active state (State B), resulting in performance degradation. The activated defects may further evolve into a recovered state (State C), which exhibits relatively stable performance during thermal treatment in the dark. Importantly, the degradation and recovery processes can occur simultaneously, allowing different defect states to co-exist. Therefore, the observed performance variations during thermal treatment are associated with the redistribution of defects among various defect states. The extent of degradation is ultimately determined by the competition between degradation and recovery rates, both of which are strongly temperature dependent. Furthermore, States B and C can also be reversed back to State An under certain light-soaking conditions.

According to the findings in earlier sections, the activation of the defects from State A to State B can be triggered by the dark annealing process at a moderate temperature (e.g. 150 °C). The activated defects can be temporarily returned to State A via a brief light soaking process at room temperature. However, the subsequent dark conditions may lead to partial degradation again. Moreover, under the dark annealing process, State B can also be recovered to State C, which remains relatively stable during further thermal treatment. However, applying a one-sun light soaking at a relatively higher temperature (e.g. 350 °C) may destabilize the inactive defects and reactivate them back to State A, resulting in renewed degradation when subjected to the thermal test again.

Although further investigation is required to fully understand this novel defect, some hypotheses can be proposed based on the current experimental results. The degradation and recovery trends are quite similar to those previously observed in light- and elevated temperature-induced degradation (LeTID), carrier-induced degradation (CID) and ultraviolet-induced degradation (UVID) studies [26,50–55], suggesting that hydrogen (H) may play a crucial role. Hydrogen is released from the passivation layer during the firing process and may interact with pre-existing impurities (e.g. carbon, oxygen) or even vacancies [56–59] to form recombination-active complexes under certain conditions (dark annealing in our case). Additionally, hydrogen may also accumulate at the interfaces, resulting in increased recombination [60]. Moreover, the hydrogen-induced recombination (HIR) theory proposed by Wenham et al. [61] suggests that even high concentrations of H alone can lead to

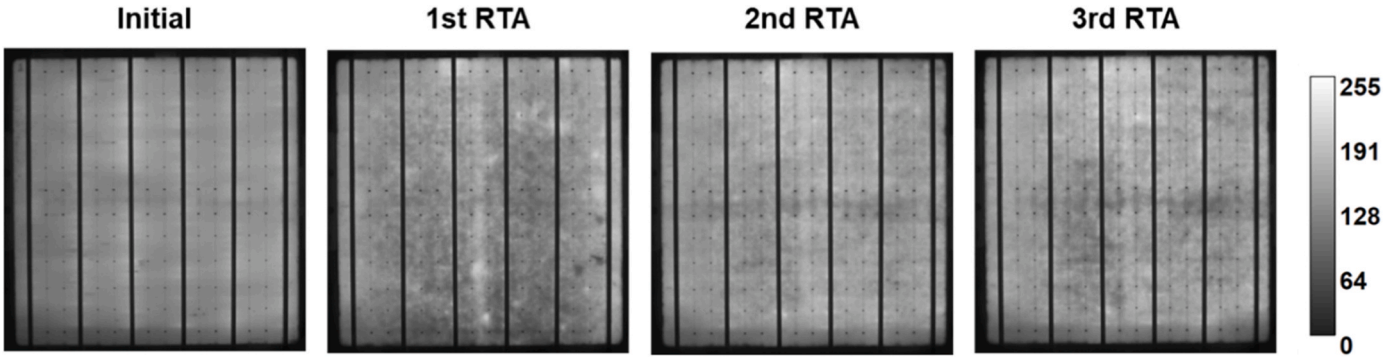


**Fig. 9.** EL Images of samples at the initial state and after 3 steps of the RTA process, as outlined in Fig. 1 (c).

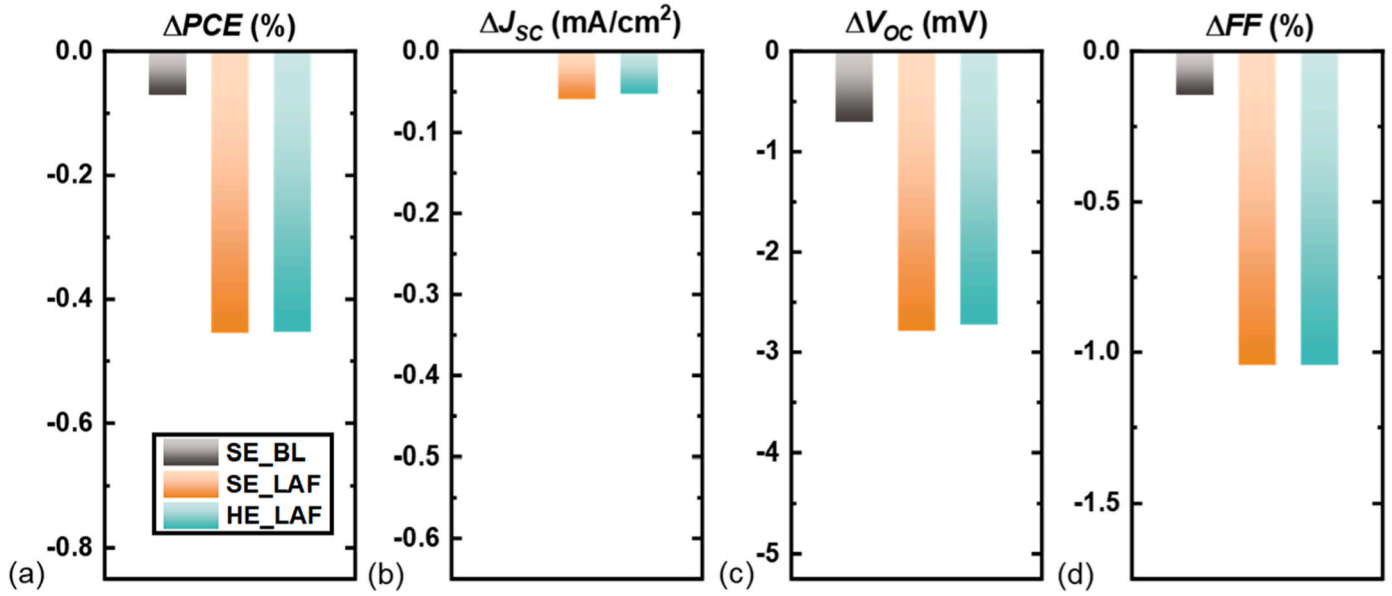


**Fig. 10.** Absolute variations of one-sun (a) *PCE*, (b) $J_{sc}$, (c) $V_{oc}$, and (d) *FF* values of the SE_BL, SE_LAF and HE_LAF solar cells after 15 min of 150 °C dark annealing.

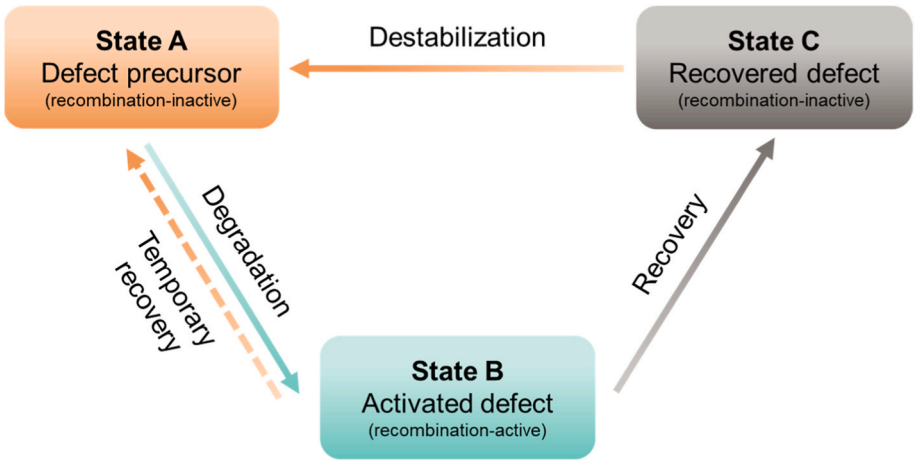


**Fig. 11.** The proposed three-state defect model and pathways for the degradation and regeneration in LAF TOPCon solar cells.

degradation in Si solar cells. The continuous charge state transition between $H^0$ and $H^+/H^-$ facilitates the recombination due to the loss of electrons and holes during the process. Furthermore, Nickel et al. [62] demonstrated that hydrogen atoms can form crystallographic defects. The active defects may then be dispersed or passivated by the subsequent thermal or illumination process, resulting in performance recovery. These mechanisms align well with the degradation and recovery behaviour observed in our study.

Fig. 10 illustrates that the defect induced under moderate thermal conditions is strongly linked to, or at least boosted by, the utilization of the LAF technique. Therefore, although the three-state defect model can qualitatively describe defect dynamics in both LAF and BL TOPCon cells, the extent and kinetics of these transitions differ due to the distinct hydrogen behaviour introduced by the LAF process. In addition to the firing process, the LAF technology introduces a high-density laser scanning process combined with an applied reverse bias. Therefore, the high intensity of laser illumination and induced localized heating [10] during the process may release additional H into Si. Moreover, a previous study has reported that hydrogen can migrate from the n-type bulk to the p-type emitter region under reverse bias [23]. Consequently, a high concentration of H may accumulate at the emitter region after the LAF process, leading to thermal-induced recombination at the front, which is consistent with the deduction from Fig. 4 (b). Therefore, although the $SiN_x$ passivation layers used in both LAF and BL TOPCon cells are identical and provide similar initial hydrogen reservoirs, the LAF process can significantly alter the hydrogen distribution. This redistribution of hydrogen also explains why the LAF-processed TOPCon cells show higher CTM loss and more severe thermal degradation than the BL ones shown in Fig. 10. Additionally, the application of the LAF technique allows for the use of significantly higher emitter sheet resistances in TOPCon solar cells, leading to a correspondingly thinner emitter region [9]. Therefore, the site of the induced recombination might be close or even at the p-n junction. This could lead to $J_{02}$-like recombination [33], which significantly reduces the *pFF* and *PCE* as shown in Fig. 3.

Moreover, the contact degradation during the high-temperature RTA may also be caused by the accumulation of hydrogen. Previous work [23] has shown that a 400 °C dark annealing under reverse bias can significantly increase the contact resistance of LAF cells, suggesting a potential high-temperature degradation mechanism involving hydrogen as well. During the high-temperature process, hydrogen may accumulate at the metal–Si interface, contributing to increased contact resistance

[63–65]. Notably, the contact formed by LAF process features a significantly lower contact fraction between the metal and Si [19], potentially exacerbating the contact properties and increasing the interface sensitivity to hydrogen accumulation. The following LAF process may help disperse the accumulated hydrogen from the metal-Si interface, thereby restoring the contact performance. The reduced extent of degradation observed in subsequent RTA tests may be attributed to hydrogen effusion during the first cycle of RTA and LAF treatment. The current hypotheses are just based on the electrical characterization results, more detailed material-level characterization is expected in future work to further verify the variations of the hydrogen state induced by LAF process.

#### 3.5.2. Other possible mechanisms

The degradation under moderate-temperature annealing may also be associated with some metallic impurities potentially present in the precursor or pastes of the LAF TOPCon solar cells, which might be either activated or introduced during the LAF process. Metal precipitates can diffuse into Si [66,67], form complexes with interstitial impurities, including H, during the high-temperature process. Subsequent thermal treatment may cause the complex dissociation and also stabilization of interstitials [68,69], resulting in the degradation and recovery of the cell performance.

Regarding the contact degradation after the RTA process, Xie et al. [22] suggested that high-temperature firing melts the glass frit in the paste and disrupts the carrier collection path. The LAF process then reforms the contact structure, thereby restoring carrier collection capability. While this model effectively explains the observed contact degradation and recovery, it does not fully account for the reduced contact deterioration after repeated RTA processes, as shown in Figs. 8 and 9. Therefore, a refined mechanism is still needed.

In general, current collection between the metal and silicon can be understood via two mechanisms: (1) Direct contact [70], where carriers are transported through contact between the metal bulk and the silicon, and (2) Tunnelling transport [71], where carriers pass through nano-Ag colloids embedded in the interfacial glass layer. Due to the utilization of customized front paste and LAF technology, the direct carrier collection in LAF cells predominantly depends on a limited number of direct contact points at the peaks of the surface pyramid, while the carriers at most areas (pyramid slopes) are transported via tunnelling [8,14,19]. This unique structure effectively preserves the passivation layer, leading to improved $V_{oc}$, but also introduces potential risks in the thermal stability of the metal–Si contact.

During high-temperature RTA, the low-melting-point glass frit softens [72], potentially altering the pre-formed interface glass structure [73], while the metal–Si alloy contact remains relatively intact due to the higher eutectic temperature [74,75]. As a result, the tunnelling pathway for carrier collection may be destroyed, forcing the cell to rely primarily on direct contact, which leads to a substantial increase in contact resistance. A subsequent LAF step can reconstruct the tunnelling channels by reforming nano-Ag colloids within the glass. At the same time, some additional direct contact points between metal and silicon can also be introduced, supported by observations of increased corrosion at pyramid tips after a second LAF process [22]. Hence, although a second RTA again disrupts the tunnelling path, the larger number of remaining direct contacts helps limit the rise in contact resistance. The similar extent of degradation observed following the third RTA can be attributed to the saturation of direct contact formation following the initial RTA and LAF cycle.

## 4. Conclusion

Laser-assisted firing (LAF) is already widely used in the PV industry. In this work, the stability of the LAF TOPCon solar cells under both moderate and high thermal conditions is assessed. Under moderate thermal stress (temperatures used during module fabrication), no degradation is observed after soldering, but lamination results in a ~0.29 % absolute *PCE* loss, mainly due to a ~0.66 % *FF* loss and a slight (~1.5 mV) $V_{oc}$ drop. A 10-s 350 °C one-sun light soaking and a 15-min 150 °C dark annealing simulates the soldering and lamination process, and successfully reproduces the degradation. Subsequent annealing then gradually restores the performance of degraded samples. Higher annealing temperatures (180 °C and 250 °C) accelerate both degradation and recovery, indicating competing degradation and recovery mechanisms.

Characterization reveals $J_{02}$-like recombination probably in the space charge region as the primary cause, supported by injection-dependent PL images taken under short- and open-circuit conditions. A 250 °C pre-annealing stabilizes the cells, but soldering can reactivate defects. Cycling tests confirm that the destabilization process reactivates the passivated defects, instead of generating new defects from a reservoir. A 1-min exposure to one-sun illumination at room temperature fully restores cell performance, indicating a self-healing effect under field conditions. Nevertheless, partial degradation can occur during dark storage, highlighting the importance of accounting for both thermal and illumination histories of modules in reliability assessments. After high-temperature RTA (450 °C), contact degradation leads to a notable increase in $R_s$, resulting in a ~21.6 % *FF* and ~6.7 % *PCE* loss. Recovery is achieved via the subsequent LAF process, with reduced degradation in repeated cycles.

A three-state defect model is proposed, involving transitions between a defect precursor state, a recombination-active state and a recovered state. Hydrogen introduced during LAF is identified as a likely contributor causing recombination at the front junction under moderate stress and/or accumulating at contacts under high temperatures. Metal precipitates and contact restructuring in the LAF cells may also play roles in the observed degradation and recovery. While further investigation is needed, this study offers crucial insights into LAF-induced reliability challenges.

## CRediT authorship contribution statement

**Xutao Wang:** Writing – review & editing, Writing – original draft, Visualization, Validation, Software, Methodology, Investigation, Formal analysis. **Jing Yuan:** Investigation, Formal analysis, Data curation. **Jianjun Nie:** Investigation, Formal analysis, Data curation. **Yan Zhu:** Methodology, Investigation, Formal analysis. **Xiaoyan Zhang:** Investigation, Data curation. **Ting Gou:** Investigation, Data curation. **Daoxian Li:** Investigation, Data curation. **Weiguang Yang:** Project administration, Methodology, Investigation, Formal analysis. **Feng Li:** Methodology, Investigation. **Xinyuan Wu:** Writing – review & editing, Investigation, Formal analysis. **Bram Hoex:** Writing – review & editing, Supervision, Project administration, Methodology, Investigation, Funding acquisition, Formal analysis, Conceptualization.

## Declaration of competing interest

The authors declare the following financial interests/personal relationships which may be considered as potential competing interests: Bram Hoex reports financial support was provided by Australian Centre for Advanced Photovoltaics. Bram Hoex reports financial support was provided by Australian Renewable Energy Agency. If there are other authors, they declare that they have no known competing financial interests or personal relationships that could have appeared to influence the work reported in this paper.

## Acknowledgments

The work is supported by the Australian Centre for Advanced Photovoltaics (ACAP) and received funding from the Australian Renewable Energy Agency (ARENA). The authors gratefully acknowledge the support from the Australian Government's Trailblazer for Recycling &

Clean Energy (TRaCE) program, led by UNSW and the University of Newcastle. The authors express their gratitude to the valuable support from the UNSW LDOT team at both the Solar Industrial Research Facility (SIRF) and the Tyree Energy Technologies Building (TETB). Xutao Wang acknowledges a TRaCE Scholarship and a University International Postgraduate Award (UIPA) Scholarship, provided by UNSW.

## Data availability

Data will be made available on request.

## References

[1] VDMA, International technology roadmap for photovoltaic. https://www.vdma.eu/en-GB/international-technology-roadmap-photovoltaic, 2025.
[2] X. Li, Q. Wang, X. Dong, J. Li, X. Zhang, N. Yuan, L. Li, J. Ding, Optimization of efficiency enhancement of TOPCon cells with boron selective emitter, Sol. Energy Mater. Sol. Cell. 263 (2023) 112585, https://doi.org/10.1016/j.solmat.2023.112585.
[3] H. Du, X. Zhang, W. Liu, Z. Liu, H. Pu, Z. Ying, X. Yang, Z. Yang, Y. Zeng, J. Ye, High-performance boron emitters for tunnel oxide passivating contact solar cells enabled by multi-layer PECVD-deposited boron source structures, Chem. Eng. J. 515 (2025) 163487, https://doi.org/10.1016/j.cej.2025.163487.
[4] B. Liao, S. Ma, R.J. Yeo, X. Wu, S. Zou, X. Su, W. Shen, G. Xing, B. Hoex, Novel Nano-Pyramid/Polish hybrid morphology designed for high-efficiency passivated contact solar cells, Prog. Photovoltaics Res. Appl. n/a (n.d.). https://doi.org/10.1002/pip.70002.
[5] W. Chen, W. Liu, L. Yuan, J. Cao, C. Ma, Y. Wan, Fabrication of selective boron emitters for TOPCon solar cells using boron-doped amorphous silicon as diffusion source, Sol. Energy 299 (2025) 113706, https://doi.org/10.1016/j.solener.2025.113706.
[6] J. Feng, B. Yu, Y. He, A. Lv, J. Fan, L. Yang, Z. Xia, Z. Li, X. Meng, F. Jiang, G. Xing, J. Yu, Enabling 95 % bifaciality of efficient TOPCon solar cells by rear-side selective sunken pyramid structure and zebra-crossing passivation contact, Sol. Energy Mater. Sol. Cell. 292 (2025) 113809, https://doi.org/10.1016/j.solmat.2025.113809.
[7] M.A. Green, E.D. Dunlop, M. Yoshita, N. Kopidakis, K. Bothe, G. Siefer, X. Hao, J. Y. Jiang, Solar cell efficiency tables (Version 66), Prog. Photovoltaics Res. Appl. 33 (2025) 795–810, https://doi.org/10.1002/pip.3919.
[8] Q. Wang, K. Guo, S. Gu, W. Wu, L. Li, D.E. Erişen, G. Yong, J. Ding, Impact of laser-enhanced contact optimization on n-TOPCon solar cells' performance and efficiency: experimental and simulated insights, Sol. Energy Mater. Sol. Cell. 285 (2025) 113526, https://doi.org/10.1016/j.solmat.2025.113526.
[9] S. Chen, C. Guo, Z. Liu, Z. Yang, Y. Zeng, W. Zhang, J. Ye, Mechanisms and strategies for laser-enhanced contact optimization in tunnel oxide passivating contact solar cells with ultra-high sheet resistance emitters, Chem. Eng. J. 513 (2025) 162979, https://doi.org/10.1016/j.cej.2025.162979.
[10] H. Höffler, F. Simon, E. Krassowski, J. Greulich, Understanding current paths and temperature distributions during 'Laser Enhanced Contact Optimization' (LECO), in: AIP Conference Proceedings, 2826, 2023 040002, https://doi.org/10.1063/5.0141008.
[11] T. Fellmeth, H. Höffler, S. Mack, E. Krassowski, K. Krieg, B. Kafle, J. Greulich, Laser-enhanced contact optimization on iTOPCon solar cells, Prog. Photovoltaics Res. Appl. 30 (2022) 1393–1399, https://doi.org/10.1002/pip.3598.
[12] A. Mette, S. Hörnlein, F. Stenzel, R. Hönig, I. Höger, M. Schaper, K. Petter, M. Junghänel, C. Klenke, A. Weihrauch, H.-C. Ploigt, O. Kwon, A. Schönmann, O. Tobail, K. Kim, A. Schwabedissen, M. Kauert, K. Duncker, B. Faulwetter-Quandt, J. Scharf, J. Cieslak, F. Kersten, B. Lee, S.T. Kristensen, O. Schnelting, C. Baer, M. Queck, G. Zimmermann, L. Burtone, L. Niebergall, M. Schütze, S. Schulz, M. Fischer, S. Peters, F. Fertig, J.W. Müller, Q.ANTUM NEO with LECO Exceeding 25.5 % cell Efficiency, Sol. Energy Mater. Sol. Cell. 277 (2024) 113110, https://doi.org/10.1016/j.solmat.2024.113110.
[13] X. Wang, J. Yuan, X. Wu, J. Nie, Y. Zhang, X. Zhang, W. Yang, F. Li, B. Hoex, Higher-efficiency TOPCon solar cells in mass production enabled by laser-assisted firing: advanced loss analysis and near-term efficiency potential, Prog. Photovoltaics Res. Appl. 33 (2025) 771–781, https://doi.org/10.1002/pip.3921.
[14] Y. Fan, S. Zou, Y. Zeng, L. Dai, Z. Wang, Z. Lu, H. Sun, X. Zhou, B. Liao, X. Su, Investigation of the Ag–Si contact characteristics of boron emitters for n-Tunnel oxide-passivated contact solar cells metallized by laser-assisted current injection treatment, Sol. RRL 8 (2024) 2400268, https://doi.org/10.1002/solr.202400268.
[15] R. Zhou, Y. Li, Z. Zhang, W. Tan, Z. Chen, Y. Lin, F. Pan, Nano-size Joule-heating to achieve low-ohmic Ag–Si contact on boron emitters of n-TOPCon solar cells, Small 21 (2025) 2409628, https://doi.org/10.1002/smll.202409628.
[16] S. Großer, E. Krassowski, S. Swatek, H. Zhao, C. Hagendorf, Microscale contact formation by laser enhanced contact optimization, IEEE J. Photovoltaics 12 (2022) 26–30, https://doi.org/10.1109/JPHOTOV.2021.3129362.
[17] J.M. Greulich, C. Leon, S. Mack, D. Ourinson, J.D. Huyeng, S. Rein, Microstructure analysis of current-fired contacts on TOPCon layers, Sol. RRL 9 (2025) 2500197, https://doi.org/10.1002/solr.202500197.
[18] S. Lange, S. Swatek, M. Turek, S. Großer, E. Krassowski, J. Hoß, S.S. Kalaghichi, J. Lossen, Efficiency improvement and microstructural working principle of LECO on the n-TOPCon rear side of industrial-like TOPCon solar cells, Sol. Energy Mater. Sol. Cell. 292 (2025) 113795, https://doi.org/10.1016/j.solmat.2025.113795.
[19] Q. Wang, K. Guo, S. Gu, W. Huang, W. Wu, J. Ding, Investigation on effects of the laser-enhanced contact optimization process with Ag paste in a boron emitter for n-TOPCon solar cell, Prog. Photovoltaics Res. Appl. 33 (2025) 294–308, https://doi.org/10.1002/pip.3854.
[20] X. Wu, W. Wu, Y. Zhang, J. Fu, X. Wang, J. Li, W. Yang, F. Li, L. Lv, J.Y. Jiang, B. Hoex, Is TOPCon ready for EVA? Insights from damp heat testing of glass-backsheet modules, Sol. Energy Mater. Sol. Cell. 288 (2025) 113650, https://doi.org/10.1016/j.solmat.2025.113650.
[21] X. Wu, X. Wang, W. Yang, J. Nie, J. Yuan, M.U. Khan, A. Ciesla, C. Sen, Z. Qiao, B. Hoex, Enhancing the reliability of TOPCon technology by laser-enhanced contact firing, Sol. Energy Mater. Sol. Cells 271 (2024) 112846, https://doi.org/10.1016/j.solmat.2024.112846.
[22] Y.-B. Xie, C.-Y. Fang, D.-S. Chen, Y. He, S.-H. Huang, Influence of laser induced sintering on contact performance of TOPCon solar cells, Acta Phys. Sin. 73 (2024) 248801, https://doi.org/10.7498/aps.73.20241372.
[23] Y. Xiong, T.O.A. Fattah, K. Okamoto, R.S. Bonilla, A failure mode affecting the reliability of LECO-treated high-efficiency TOPCon solar cells, Sol. RRL 9 (2025) 2500151, https://doi.org/10.1002/solr.202500151.
[24] C.A. Schneider, W.S. Rasband, K.W. Eliceiri, NIH image to ImageJ: 25 years of image analysis, Nat. Methods 9 (2012) 671–675, https://doi.org/10.1038/nmeth.2089.
[25] K. Hong Min, H. Song, M. Gu Kang, S. Hee Lee, S. Park, Double-diode model carrier lifetime-based internal recombination parameter analysis and efficiency prediction of crystalline Si solar cells, Sol. Energy 277 (2024) 112697, https://doi.org/10.1016/j.solener.2024.112697.
[26] D. Chen, P. Hamer, M. Kim, C. Chan, A. Ciesla nee Wenham, F. Rougieux, Y. Zhang, M. Abbott, B. Hallam, Hydrogen-induced degradation: explaining the mechanism behind light- and elevated temperature-induced degradation in *n*- and *p-type* silicon, Sol. Energy Mater. Sol. Cell. 207 (2020) 110353, https://doi.org/10.1016/j.solmat.2019.110353.
[27] C. Vargas, G. Coletti, C. Chan, D. Payne, Z. Hameiri, On the impact of dark annealing and room temperature illumination on *p*-type multicrystalline silicon wafers, Sol. Energy Mater. Sol. Cell. 189 (2019) 166–174, https://doi.org/10.1016/j.solmat.2018.09.018.
[28] C. Vargas, S. Nie, D. Chen, C. Chan, B. Hallam, G. Coletti, Z. Hameiri, Degradation and recovery of n-Type multi-crystalline silicon under illuminated and dark annealing conditions at moderate temperatures, IEEE J. Photovoltaics 9 (2019) 355–363, https://doi.org/10.1109/JPHOTOV.2018.2885711.
[29] H. Stolzenburg, A. Fell, F. Schindler, W. Kwapil, A. Richter, P. Baliozian, M. C. Schubert, Edge recombination analysis of silicon solar cells using photoluminescence measurements, in: AIP Conference Proceedings, 2147, 2019 020017, https://doi.org/10.1063/1.5123822.
[30] J. Wong, R. Sridharan, V. Shanmugam, Quantifying edge and peripheral recombination losses in industrial silicon solar cells, IEEE Trans. Electron. Dev. 62 (2015) 3750–3755, https://doi.org/10.1109/TED.2015.2480089.
[31] F. Gérenton, J. Eymard, S. Harrison, R. Clerc, D. Muñoz, Analysis of edge losses on silicon heterojunction half solar cells, Sol. Energy Mater. Sol. Cell. 204 (2020) 110213, https://doi.org/10.1016/j.solmat.2019.110213.
[32] A. Fell, J. Schön, M. Müller, N. Wöhrle, M.C. Schubert, S.W. Glunz, Modeling edge recombination in silicon solar cells, IEEE J. Photovoltaics 8 (2018) 428–434, https://doi.org/10.1109/JPHOTOV.2017.2787020.
[33] E. Resmi, K.P. Sreejith, A. Kottantharayil, Analysis of variation in recombination characteristics due to light and heat in industrial silicon solar cells, Sol. Energy 252 (2023) 127–133, https://doi.org/10.1016/j.solener.2023.01.053.
[34] D. Macdonald, A. Cuevas, Reduced fill factors in multicrystalline silicon solar cells due to injection-level dependent bulk recombination lifetimes, Prog. Photovoltaics Res. Appl. 8 (2000) 363–375, https://doi.org/10.1002/1099-159X(200007/08)8:4%253C363::AID-PIP328%253E3.0.CO;2-Y.
[35] H. Hieslmair, J. Appel, J. Kasthuri, J. Guo, B. Johnson, J. Binns, Impact of the injection-level-dependent lifetime on Voc, FF, ideality m, J02, and the dim light response in a commercial PERC cell, Prog. Photovoltaics Res. Appl. 24 (2016) 1448–1457, https://doi.org/10.1002/pip.2792.
[36] A.G. Aberle, S.J. Robinson, A. Wang, J. Zhao, S.R. Wenham, M.A. Green, High-efficiency silicon solar cells: full factor limitations and non-ideal diode behaviour due to voltage-dependent rear surface recombination velocity, Prog. Photovoltaics Res. Appl. 1 (1993) 133–143, https://doi.org/10.1002/pip.4670010204.
[37] W. Shockley, The theory of p-n junctions in semiconductors and p-n junction transistors, Bell Syst. Tech. J. 28 (1949) 435–489, https://doi.org/10.1002/j.1538-7305.1949.tb03645.x.
[38] C. Shen, K. Wang, M.A. Green, Fast separation of front and bulk defects via photoluminescence on silicon solar cells, Sol. Energy Mater. Sol. Cell. 128 (2014) 260–263, https://doi.org/10.1016/j.solmat.2014.05.029.
[39] W. Luo, Y.S. Khoo, J.P. Singh, J.K.C. Wong, Y. Wang, A.G. Aberle, S. Ramakrishna, Investigation of potential-induced degradation in n-PERT bifacial silicon Photovoltaic modules with a Glass/Glass structure, IEEE J. Photovoltaics 8 (2018) 16–22, https://doi.org/10.1109/JPHOTOV.2017.2762587.
[40] C. Sen, M. Kim, D. Chen, U. Varshney, S. Liu, A. Samadi, A. Ciesla, S.R. Wenham, C. E. Chan, C. Chong, M.D. Abbott, B.J. Hallam, Assessing the impact of thermal profiles on the elimination of Light- and elevated-temperature-induced degradation, IEEE J. Photovoltaics 9 (2019) 40–48, https://doi.org/10.1109/JPHOTOV.2018.2874769.
[41] H.C. Sio, D. Kang, X. Zhang, J. Yang, J. Jin, D. Macdonald, The role of dark annealing in light and elevated temperature induced degradation in p-Type Mono-

Like silicon, IEEE J. Photovoltaics 10 (2020) 992–1000, https://doi.org/10.1109/JPHOTOV.2020.2993653.
[42] S. Cheng, F. Ji, C. Zhou, J. Zhu, R. Søndenå, W. Wang, D. Hu, Kinetics of light and elevated temperature-induced degradation in cast mono p-type silicon, Sol. Energy 224 (2021) 1000–1007, https://doi.org/10.1016/j.solener.2021.06.054.
[43] M. Yli-Koski, M. Serué, C. Modanese, H. Vahlman, H. Savin, Low-temperature dark anneal as pre-treatment for LeTID in multicrystalline silicon, Sol. Energy Mater. Sol. Cell. 192 (2019) 134–139, https://doi.org/10.1016/j.solmat.2018.12.021.
[44] T.H. Fung, M. Kim, D. Chen, C.E. Chan, B.J. Hallam, R. Chen, D.N.R. Payne, A. Ciesla, S.R. Wenham, M.D. Abbott, A four-state kinetic model for the carrier-induced degradation in multicrystalline silicon: introducing the reservoir state, Sol. Energy Mater. Sol. Cell. 184 (2018) 48–56, https://doi.org/10.1016/j.solmat.2018.04.024.
[45] Z. Li, K. Yu, Q. Zhu, L. Wang, Y. Chen, J. Huang, G. Zhou, X. Sun, J. Gao, L. Zhou, UVID of TOPCon solar cells: effect of the front passivation Al2O3 layer thickness and recovery by different processes, Sol. Energy Mater. Sol. Cell. 289 (2025) 113691, https://doi.org/10.1016/j.solmat.2025.113691.
[46] F.T. Thome, P. Meßmer, S. Mack, E. Schnabel, F. Schindler, W. Kwapil, M. C. Schubert, UV-Induced degradation of industrial PERC, TOPCon, and HJT solar cells: the next big reliability challenge? Sol. RRL 8 (2024) 2400628 https://doi.org/10.1002/solr.202400628.
[47] P. Gebhardt, E. Fokuhl, S.S. Mujumdar, H. Frey, A. Beinert, A. Stöhr, M. Kaiser, I. Hädrich, Stabilization procedures for TOPCon modules after UV-Induced degradation. https://doi.org/10.24406/publica-4677, 2025.
[48] D. Sperber, A. Herguth, G. Hahn, A 3-state defect model for light-induced degradation in boron-doped float-zone silicon, Phys. Status Solidi Rapid Res. Lett. 11 (2017) 1600408, https://doi.org/10.1002/pssr.201600408.
[49] K. Krauß, A.A. Brand, F. Fertig, S. Rein, J. Nekarda, Fast regeneration processes to avoid light-induced degradation in multicrystalline silicon solar cells, IEEE J. Photovoltaics 6 (2016) 1427–1431, https://doi.org/10.1109/JPHOTOV.2016.2598273.
[50] B. Hammann, P. Vieira Rodrigues, N. Aßmann, W. Kwapil, F. Schindler, M. C. Schubert, S.W. Glunz, Deciphering the role of hydrogen in the degradation of silicon solar cells under light and elevated temperature, Sol. RRL 8 (2024) 2400457, https://doi.org/10.1002/solr.202400457.
[51] D. Chen, M. Kim, B.V. Stefani, B.J. Hallam, M.D. Abbott, C.E. Chan, R. Chen, D.N. R. Payne, N. Nampalli, A. Ciesla, T.H. Fung, K. Kim, S.R. Wenham, Evidence of an identical firing-activated carrier-induced defect in monocrystalline and multicrystalline silicon, Sol. Energy Mater. Sol. Cell. 172 (2017) 293–300, https://doi.org/10.1016/j.solmat.2017.08.003.
[52] D. Chen, P.G. Hamer, M. Kim, T.H. Fung, G. Bourret-Sicotte, S. Liu, C.E. Chan, A. Ciesla, R. Chen, M.D. Abbott, B.J. Hallam, S.R. Wenham, Hydrogen induced degradation: a possible mechanism for light- and elevated temperature- induced degradation in n-type silicon, Sol. Energy Mater. Sol. Cell. 185 (2018) 174–182, https://doi.org/10.1016/j.solmat.2018.05.034.
[53] C. Chan, T.H. Fung, M. Abbott, D. Payne, A. Wenham, B. Hallam, R. Chen, S. Wenham, Modulation of carrier-induced defect kinetics in multi-crystalline silicon PERC cells through Dark Annealing, Sol. RRL 1 (2017) 1600028, https://doi.org/10.1002/solr.201600028.
[54] S. Razzaq, L. Wei, R. Jiao, C. Cheng, H. Yuting, L. Lin, Y. Po-Chuan, A. Asghar, C. Lou, Enhancing UV light stability in commercial silicon HJT solar cells and modules, Sol. Energy 298 (2025) 113735, https://doi.org/10.1016/j.solener.2025.113735.
[55] J. Yang, Y. Tang, C. Zhou, S. Chen, S. Cheng, L. Wang, S. Zhou, X. Jia, W. Wang, X. Xu, J. Xiao, W. Wei, Unveiling the mechanism of ultraviolet-induced degradation in silicon heterojunction solar cells, Sol. Energy Mater. Sol. Cell. 276 (2024) 113062, https://doi.org/10.1016/j.solmat.2024.113062.
[56] M. Vaqueiro-Contreras, V.P. Markevich, M.P. Halsall, A.R. Peaker, P. Santos, J. Coutinho, S. Öberg, L.I. Murin, R. Falster, J. Binns, E.V. Monakhov, B. G. Svensson, Powerful recombination centers resulting from reactions of hydrogen with carbon–oxygen defects in n-type Czochralski-grown silicon, Phys. Status Solidi Rapid Res. Lett. 11 (2017) 1700133, https://doi.org/10.1002/pssr.201700133.
[57] P. Santos, J. Coutinho, S. Öberg, M. Vaqueiro-Contreras, V.P. Markevich, M. P. Halsall, A.R. Peaker, Theory of a carbon-oxygen-hydrogen recombination center in n-type Si, Phys. Status Solidi 214 (2017) 1700309, https://doi.org/10.1002/pssa.201700309.
[58] I.L. Kolevatov, B.G. Svensson, E.V. Monakhov, Correlated annealing and formation of vacancy-hydrogen related complexes in silicon, J. Phys. Condens. Matter 31 (2019) 235703, https://doi.org/10.1088/1361-648X/ab0bf2.
[59] I.L. Kolevatov, P.M. Weiser, E.V. Monakhov, B.G. Svensson, Interaction between hydrogen and vacancy defects in crystalline Silicon, Phys. Status Solidi 216 (2019) 1800670, https://doi.org/10.1002/pssa.201800670.
[60] K. Kim, R. Chen, D. Chen, P. Hamer, A. Ciesla nee Wenham, S. Wenham, Z. Hameiri, Degradation of surface passivation and bulk in p-Type monocrystalline silicon wafers at elevated temperature, IEEE J. Photovoltaics 9 (2019) 97–105, https://doi.org/10.1109/JPHOTOV.2018.2878791.
[61] A.C. née Wenham, S. Wenham, R. Chen, C. Chan, D. Chen, B. Hallam, D. Payne, T. Fung, M. Kim, S. Liu, S. Wang, K. Kim, A. Samadi, C. Sen, C. Vargas, U. Varshney, B.V. Stefani, P. Hamer, G. Bourret-Sicotte, N. Nampalli, Z. Hameiri, C. Chong, M. Abbott, Hydrogen-Induced degradation, in: 2018 IEEE 7th World Conference on Photovoltaic Energy Conversion (WCPEC) (A Joint Conference of 45th IEEE PVSC, 28th PVSEC & 34th EU PVSEC), 2018, pp. 1–8, https://doi.org/10.1109/PVSC.2018.8548100.
[62] N.H. Nickel, G.B. Anderson, J. Walker, Hydrogen-induced platelets in disordered silicon, Solid State Commun. 99 (1996) 427–431, https://doi.org/10.1016/0038-1098(96)00283-9.
[63] D. Liu, M. Wright, M. Goodarzi, P.R. Wilshaw, P. Hamer, R.S. Bonilla, Observations of contact resistance in TOPCon and PERC solar cells, Sol. Energy Mater. Sol. Cell. 246 (2022) 111934, https://doi.org/10.1016/j.solmat.2022.111934.
[64] P. Hamer, C. Chan, R.S. Bonilla, B. Hallam, G. Bourret-Sicotte, K.A. Collett, S. Wenham, P.R. Wilshaw, Hydrogen induced contact resistance in PERC solar cells, Sol. Energy Mater. Sol. Cell. 184 (2018) 91–97, https://doi.org/10.1016/j.solmat.2018.04.036.
[65] C. Chan, P. Hamer, G. Bourret-Sicotte, R. Chen, A. Ciesla, B. Hallam, D. Payne, R. S. Bonilla, S. Wenham, Instability of increased contact resistance in silicon solar cells following post-firing thermal processes, Sol. RRL 1 (2017) 1700129, https://doi.org/10.1002/solr.201700129.
[66] R. Hoenig, M. Glatthaar, F. Clement, J. Greulich, J. Wilde, D. Biro, New measurement method for the investigation of space charge region recombination losses induced by the metallization of silicon solar cells, Energy Proc. 8 (2011) 694–699, https://doi.org/10.1016/j.egypro.2011.06.203.
[67] R. Hoenig, A. Kalio, J. Sigwarth, F. Clement, M. Glatthaar, J. Wilde, D. Biro, Impact of screen printing silver paste components on the space charge region recombination losses of industrial silicon solar cells, Sol. Energy Mater. Sol. Cell. 106 (2012) 7–10, https://doi.org/10.1016/j.solmat.2012.06.040.
[68] D. Bredemeier, D. Walter, S. Herlufsen, J. Schmidt, Lifetime degradation and regeneration in multicrystalline silicon under illumination at elevated temperature, AIP Adv. 6 (2016) 035119, https://doi.org/10.1063/1.4944839.
[69] D. Chen, M. Vaqueiro Contreras, A. Ciesla, P. Hamer, B. Hallam, M. Abbott, C. Chan, Progress in the understanding of light- and elevated temperature-induced degradation in silicon solar cells: a review, Prog. Photovoltaics Res. Appl. 29 (2021) 1180–1201, https://doi.org/10.1002/pip.3362.
[70] E. Cabrera, S. Olibet, J. Glatz-Reichenbach, R. Kopecek, D. Reinke, G. Schubert, Current transport in thick film Ag metallization: direct contacts at Silicon pyramid tips? Energy Proc. 8 (2011) 540–545, https://doi.org/10.1016/j.egypro.2011.06.179.
[71] M. Pfeffer, P. Kumar, O. Eibl, High-Efficiency Crystalline-Si solar cells with screen-printed front-side metallization: a percolation model to explainthe Current path, J. Electron. Mater. 45 (2016) 5764–5772, https://doi.org/10.1007/s11664-016-4818-5.
[72] Y. Zhang, Y. Yang, J. Zheng, W. Hua, G. Chen, Thermal properties of glass frit and effects on Si solar cells, Mater. Chem. Phys. 114 (2009) 319–322, https://doi.org/10.1016/j.matchemphys.2008.09.011.
[73] A. Peral, A. Dastgheib-Shirazi, V. Fano, J.C. Jimeno, G. Hahn, C. del Cañizo, Impact of extended contact cofiring on multicrystalline silicon solar cell parameters, IEEE J. Photovoltaics 7 (2017) 91–96, https://doi.org/10.1109/JPHOTOV.2016.2621342.
[74] R.W. Olesinski, A.B. Gokhale, G.J. Abbaschian, The Ag-Si (Silver-Silicon) system, Bullet. Alloy Phase Diag. 10 (1989) 635–640, https://doi.org/10.1007/BF02877631.
[75] Pooja Seema, S. Kashyap, C. Shekhar, Thermodynamic modelling of Ag–Si nanophase diagram including shape effect, J. Nanoparticle Res. 26 (2024) 1–10, https://doi.org/10.1007/s11051-024-06080-6.